Slip of gels in colloid-polymer mixtures under shear

Soft Matter

RSC Publishing

PAPER

View Article Online
View Journal | View Issue

Slip of gels in colloid–polymer mixtures under shear†

Cite this: *Soft Matter*, 2013, **9**, 3237

Pierre Ballesta,*[a] Nick Koumakis,[a] Rut Besseling,[c] Wilson C. K. Poon[b] and George Petekidis*[a]

Received 14th November 2012
Accepted 15th January 2013

DOI: 10.1039/c3sm27626k

www.rsc.org/softmatter

We investigate the time-dependent rheology and slip behaviour of colloidal gels formed under polymer-induced depletion attraction. The shape of the flow curves at low applied shear rates is suggestive of slip, which we confirm using confocal imaging. Time-dependent linear viscoelastic measurements show an unexpected drop of the elastic modulus below the viscous one after a critical time. We present a dynamic phase diagram characterizing the dependence of slip on polymer concentration and colloid volume fraction. Confocal imaging links slip to the restructuring of clusters with time, which leads to a reduction of the number of contacts between the colloidal network and the rheometer surfaces. Such behaviour is shear rate dependent and correlated to changes in the gel structure, which changed from independent small aggregates at high shear rates to percolated clusters at low shear rates.

1 Introduction

A wide range of complex nanostructured materials exhibits wall slip under shear, which affects both rheological measurements and industrial processes. The importance of the former has long been realized.[1] Slip occurs in the flow of simple liquids and complex multiphase fluids.[2,3] In the former, slip is related to molecular interactions at lyophobic or superhydrophobic surfaces.[4–6] In complex fluids, slip is the result of the interaction between mesoscopic structural components and surfaces. Thus, in polymer melts and solutions, slip at high shear rates occurs due to conformational and dynamic changes of the chains near the wall.[7–9] Slip appears also in other complex multicomponent systems such as particle suspensions and pastes,[10–19] colloidal gels[20–25] and emulsions, foams,[26–30] and wormlike micelle solutions,[31,32] where it is detected either at low or high shear rates and often is related to shear banding.[33] Since any meaningful rheology requires knowledge of boundary effects[34] and slip affects the outcome of many industrial processes, understanding of its microscopic origins and rheological consequences is of profound importance.

Attractive particle dispersions[20,35] and emulsions[36] present similar phenomenology: shear thinning at high applied shear rates ($\dot{\gamma}$) and a drop of stress on decreasing shear rate at low $\dot{\gamma}$ attributable to wall slip. In ref. 20, the authors link the presence of a yield stress in the slipping regime to the attraction between the particle and wall. Slip was also shown recently to occur intermittently below a critical stress in different low concentration particle gels[22,23] though the exact particle–wall interaction was not explored. At $\dot{\gamma} = 0$, such systems display percolated networks of clusters. While the destruction of such networks by shear probably controls the bulk rheology, no corresponding real-time observations have been reported. Recent advances in confocal imaging rheometry[37] provide the means to make such observations, which should also shed light on the origins of slip.

A well-established way to induce attractive interactions between hard particles is by the addition of non-adsorbing polymers.[38,39] The range and strength of this depletion attraction between two hard spheres (radius R) are 'tuned' by the polymer size (*e.g.* as measured by its radius of gyration, r_g) and concentration (c_p) respectively. Extensive work has been carried out to characterize such colloid–polymer mixtures using light[40–42] neutron or X-ray scattering,[43,44] confocal imaging,[45–47] and rheology.[20,42,48,49] The equilibrium phase diagram is well understood[50] in the entire range of c_p, colloid volume fractions (ϕ) and size ratios, $\xi = r_g/R$. At high attraction strength, various long-lived metastable states exist, from low-ϕ clusters[52] and solid-like interconnected networks[47,53,54] to attractive glasses[40] observed above the hard-sphere glass transition at $\phi_g \simeq 0.59$. At a given (ϕ, ξ), there is a critical polymer concentration $c_p^{crit}(\phi)$ that separates liquid-like ($c < c_p^{crit}$) and solid-like ($c > c_p^{crit}$) metastable states.[51] We refer to solid samples with $\phi < \phi_g$ as gels while those with $\phi > \phi_g$ as glasses. While at low ϕ, gelation is due to arrested phase separation,[55–57] higher-ϕ gels are poorly understood.[58]

We study gels at intermediate ϕ (~0.4), which form percolated networks of clusters at low attraction or string like structures at higher attraction.[42,47] All our gels are stable under

[a]*IESL-FORTH and Department of Materials Science and Technology, University of Crete, 71110, Heraklion, Crete, Greece. E-mail: bpballest@aol.com; georgp@iesl.forth.gr*

[b]*SUPA and School of Physics, The University of Edinburgh, Kings Buildings, Mayfield Road, EH9 3JZ, Edinburgh, UK*

[c]*Merck Sharp and Dohme, Molenstraat 110, 5340 BH, Oss, Netherland*

† Electronic supplementary information (ESI) available. See DOI: 10.1039/c3sm27626k

gravity for days; however, numerical simulations[59] suggest a compaction of the clusters at long times induced by residual stress in the network. We study slip and micro-structural evolution at various state points using a combination of rheometry and confocal imaging. Thus we get a direct relation between the local structure of the suspension and its different behaviors under stress from solid-like plug flow with slip to liquid-like linear shear without slip. We first describe our experimental systems and set-up (Section 2) before presenting our main results (Section 3), which are discussed in terms of coupling between structure and flow localization.

2 Experimental

We used suspensions of polymethylmethacrylate (PMMA) colloids of various radii ($R = 130$–800 nm from light scattering) stabilized by a thin layer of poly-12-hydroxystearic acid (~10 nm), Table 1. The particles were suspended in different organic solvents: decalin, decalin–tetralin mixture (for refractive index matching), mixture of decalin–cycloheptylbromide (CHB) (for refractive index and density matching), octadecene (to minimize evaporation) and tetradecane. To avoid shear-induced crystallization the particles have a polydispersity $p \geq 10\%$. We estimated ϕ by assuming that a spun-down sample was at random close packing, $\phi_{rcp} = 0.67$, except for a more polydisperse sample ($p = 0.24$) where we used $\phi_{rcp} = 0.72$.[60] In an index-matched solvent, PMMA particles behave as almost perfect hard spheres,[61] but in octadecene and tetradecane the index mismatch between solvent and particles induces a small van der Waals attraction. We estimate this attraction without the polymer, U_{vdW}[62,63] at a separation of 20 nm, twice the size of the steric stabilization layer, to be $U_{vdW} \simeq 0.1\ k_BT$ in octadecene for two particles with $R = 138$ nm. Depletion attraction was induced by the addition of linear polybutadiene for suspensions in tetradecane and octadecene or polystyrene when the solvent was decalin or decalin–tetralin. The polymer–colloid size ratio ξ varied in the range 0.07–0.1.

We used stress-controlled (AR2000 TA, Anton Paar Physica MCR 501) and strain-controlled (ARES, TA) rheometers with cone–plate geometries. Confocal imaging was performed using fluorescent particles with $R = 650$ nm and $p = 7\%$ in a controlled stress rheometer (AR2000, TA Instr.) coupled to a confocal scanner (VT-Eye, Visitech Int.) *via* an adjustable arm.

Table 1 Solvent, particle radius (R) and polymer radius of gyration (r_g) both at 20 °C, polydispersity (p), and symbols used in Fig. 6

Solvent	R (nm)	r_g (nm)	p (%)	Symbol
Decalin–tetralin	140	9.6	15	●
Octadecene	138	14.1	15	●
Tetradecane	138	13	15	●
cis-Decalin	138	9.6	15	●
cis-Decalin	130	10	24	♦
Octadecene	167	14.1	12	■
Decalin–CHB	650	44	10	★

We used a cone–plate geometry (radius $r_c = 20$ mm, cone angle $\theta = 1°$) with a modified base on which a glass slide (radius 2.5 cm, thickness ~180 μm) was mounted. Movies were taken at intervals of $\delta_z = 1$–5 μm at ≤90 frame per second. In both rheometers, we imposed an applied shear rate, $\dot{\gamma}$. Each sample was rejuvenated at $\dot{\gamma} \sim 30\ s^{-1}$ for 5 min before measurements were started at $t = 0$. Although $\dot{\gamma} \sim 30\ s^{-1}$ was enough to redisperse the biggest particles, we expect that this would still leave small clusters for samples with smaller particles (since the Péclet number, Pe, see below, scales as R^3). Solvent traps were used to minimize the effect of evaporation over our measurement time of a few hours.

Three types of surfaces were used with the cone–plate geometries: (i) in closely index-matching solvents (*cis*-decalin, tetralin–decalin and decalin–cycloheptylbromide mixtures) surfaces were roughened by coating and sintering of a disordered monolayer of colloids of radius similar to those in the suspension. For the rheo-confocal experiments the bottom surface was a glass plate coated by a colloidal monolayer. (ii) For non-index matching solvents (*cis*/*trans*-decalin, octadecene, tetradecane) typically used in conventional rheological tests we used the standard rheometer tools (titanium or aluminium) with smooth surfaces where a monolayer of particles was stuck due to van der Waals forces. (iii) Finally some experiments were carried out with serrated tools consisting of a home-made cone and plate with roughness of about 500 μm, similar to commercial tools typically used to suppress slip. The home-made tools were tested and calibrated with viscous and viscoelastic standards.

To compare rheological results from samples with different R and c_p, we normalized the shear stress (σ), the loss (G'') and elastic (G') moduli using $\bar{\sigma} = \sigma R^3/k_BT$, $\bar{G}'' = G''R^3/k_BT$ and $\bar{G}' = G'R^3/k_BT$. The normalized shear rate is given by the Péclet number, $Pe = 6\pi\eta_s R^3\dot{\gamma}/k_BT$, with η_s being the viscosity of the polymer solution at concentration c_p.

3 Results and discussion

3.1 Flow curves and flow profiles

Fig. 1 shows flow curves (up and down sweeps) measured in a cone–plate geometry with smooth or serrated bottom plate (roughness ≃ 500 μm) for the same sample in tetradecane ($\phi = 0.45$, $c_p = 0.5c^*$, where c^* is the overlap concentration). The flow curves measured with serrated surfaces have a Herchel–Bulkley (HB) form,

$$\sigma = \sigma_y + \alpha\dot{\gamma}^n, \quad (1)$$

with σ_y the bulk yield stress and n an exponent (typically ranging between 0.4 and 0.7, depending on the sample and shear rate range reached). However, with smooth surfaces, the flow curve exhibits a drop in σ at low $\dot{\gamma}$ away from HB behaviour. In previous studies,[10,28,67] such behaviour signified slip. The region of the flow curve deviating from HB behaviour can be fitted by a Bingham law,

$$\sigma = \sigma_s + \eta\dot{\gamma}, \quad (2)$$

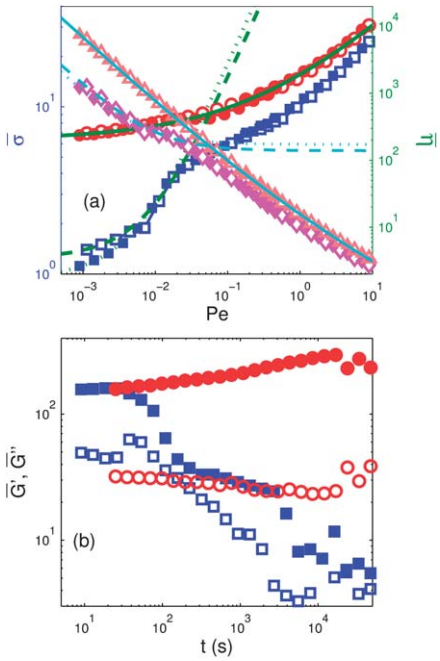

Fig. 1 Rheology data for $R = 138$ nm, $\phi = 0.45$, and $c_p = 0.5c^*$ (contact potential $U_0 = -24\ k_BT$) in tetradecane with smooth tools, where a monolayer of particles are adsorbed due to van der Waals interaction. (a) Flow curves, renormed stress $\bar{\sigma}$ *versus* Pe, with smooth (squares) and serrated (circles) plates, going from high to low (□, ○) and from low to high (■, ●) $\dot{\gamma}$, and renormed viscosity *versus* Pe with smooth (lozenges) and serrated (triangles) plates $\bar{\eta} = \bar{\sigma}/\mathrm{Pe}$, going from high to low (◇, △) and from low to high (◆, ▲). (b) Moduli at $f = 1$ Hz and $\gamma_0 = 0.1\%$ *versus* time with smooth ($\bar{G}'$ ■, $\bar{G}''$ □) and serrated plate ($\bar{G}'$ ●, $\bar{G}''$ ○). The lines in (a) correspond to an HB fit (solid line) and Bingham fit for the sweep-up (dotted line) and sweep-down (dashed line) experiments.

where σ_s is the slip stress. The linear dependence in $\dot{\gamma}$ indicates that during slip the stress is mainly transmitted through a lubrication layer, while the slip stress reflects a shear rate independent particle–wall interaction.

As it has previously been observed in attractive systems,[20] the low-shear part of the flow curves exhibits hysteresis, Fig. 1(a), with the stress when sweeping down in $\dot{\gamma}$ being larger than the stress when sweeping up. This hysteresis is due to the time-dependent rheology (thixotropy) of the system.[20] We studied this temporal evolution with small-amplitude oscillatory shear at $f = 1$ Hz and strain amplitude $\gamma_0 = 0.1\%$, Fig. 1(b). Soon after rejuvenation (typically in less than 10 s), during which the gel was shear melted ($G' < G''$), solid like behaviour was recovered ($G' < G''$), followed by a weak increase of G' and G'' typical for attractive systems due to network restructuring. However, after some time ($\approx$100 s in Fig. 1) this is followed by a decrease of both G' and G'' by more than an order of magnitude towards a state with similar G', G'' values (with large fluctuations as the limits of the transducer were reached). This decrease of the elastic modulus with time is clearly different from the aging behaviour expected in attractive systems[54,64,65] where G' increases as the cage-breaking motion slows down. However, when serrated surfaces of roughness much larger than the particle size are used, the usual time dependence is recovered with G' increasing and G'' decreasing, Fig. 1(b)).

Such time-dependence of viscoelastic properties is reminiscent of observations by Condre *et al.*[68] of sedimenting suspensions of attractive colloids. As a sample sediments, slip starts to be detected at the walls of the cell. Condre *et al.*[68] modeled this slip by Coulomb's law and showed that as the attraction between particles increased, the wall–particle network friction coefficient decreased due to an increase in cluster size. A similar time evolution of the viscoelastic properties during the collapse of weakly aggregated colloids was measured with a double Couette geometry.[69]

3.2 Structure–rheology relationship

To elucidate such behaviour and relate the mechanical properties to microscopic changes, we investigated the structure and flow profile of the gel as functions of $\dot{\gamma}$. Here we used confocal rheometry[37] of fluorescent particles ($R = 650$ nm) in an index- and density-matching solvent (decalin–CHB) at $\phi = 0.4$ and $c_p = 0.5c^*$ with a particle coated plate. A close visualization of particles near the tool's surface reveals a global slip of the network even when surfaces of roughness similar to the particles size are used. This is clearly evidenced in Fig. 2(b) in the flow profiles at $\dot{\gamma} = 0.05\ \mathrm{s}^{-1}$ and $0.01\ \mathrm{s}^{-1}$ which also show a higher shear rate for the first layer of particles close to the cone.

Below we first present microscopic flow profiles in relation with the measured flow curve revealing the dependence of the local particle velocities on the imposed shear rate. As has been

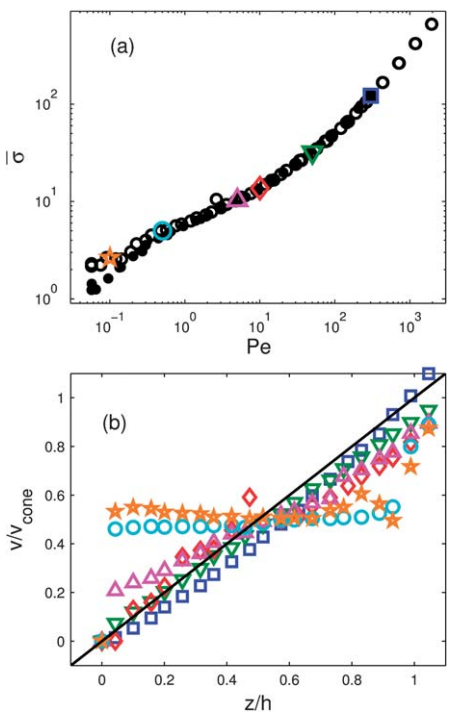

Fig. 2 (a) Flow curves for $R = 650$ nm, $\phi = 0.4$, and $U_0 = -20\ k_BT$ in density- and index-matching solvent with coated cone and plate, for decreasing (○) and increasing (●) $\dot{\gamma}$. Other symbols show where the velocity profiles in (b) were taken. (b) Velocity profiles normalized by the cone velocity *versus* the position in the gap for $\dot{\gamma} = 30\ \mathrm{s}^{-1}$ (□), $\dot{\gamma} = 5\ \mathrm{s}^{-1}$ (▽), $\dot{\gamma} = 1\ \mathrm{s}^{-1}$ (◇), $\dot{\gamma} = 0.5\ \mathrm{s}^{-1}$ (△), $\dot{\gamma} = 0.05\ \mathrm{s}^{-1}$ (○), and $\dot{\gamma} = 0.01\ \mathrm{s}^{-1}$ (⋆).

seen in hard sphere glasses,[67] the flow curve exhibits HB behaviour at higher shear rates and a drop at low shear rates (Pe < 1), Fig. 2(a). At large shear rates ($\dot{\gamma} \geq 1$ s^{-1}, Pe ≥ 10) flow profiles are approximately linear and the velocities of the fluid at the top and bottom plates are equal to those of the cone and plate, Fig. 2(b). Decreasing $\dot{\gamma}$, we find flow profiles that exhibit slip at the plate coexisting with partial shear in the bulk of the sample (see the profile at $\dot{\gamma} = 0.5$ s^{-1}, Pe = 5.5). Eventually, at $\dot{\gamma} \leq 0.05$ s^{-1} (or Pe ≤ 0.55), we find a high shear band very near the moving cone (as mentioned above), a plug flow moving at half the cone velocity, and the sample slipping at the bottom glass plate. However, it should be mentioned that during different experiments (data shown in ESI†) we also observed localized shear in the very first layers near the bottom plate.

We next discuss the gel structure as a function of shear rate and its relation with wall slip. The image stacks used to measure the velocity profiles provide such detailed microstructural information of the suspension, Fig. 3(a)–(e). These images show qualitatively that the cluster size decreases with increasing shear rates. A similar conclusion was reached by Tolpekin *et al.*[66] at very low ϕ, also using confocal microscopy. This also relates to findings by Gibaud *et al.*[22,23] that showed that at high shear rates colloidal gels fluidize and stop slipping. We extracted the cluster size, ζ, from the images using the method described in Appendix A, Fig. 3(f). Combining visual inspection of the confocal movies under shear, their analysis yielding the cluster size ζ and the flow profiles, we may conclude the following: at the lowest shear rates (Pe $\lesssim 1$), particles form interconnected clusters of about 8–9 particles diameter while the flow profile reveals a plug flow with small sheared regions near the cone (Fig. 2(b)). Increasing $\dot{\gamma}$, the onset of local shear corresponds to the presence of almost-independent clusters of about 4–5 particles diameter. A network is still present but the breaking and recombination process is fast enough to allow for a linear flow profile to be achieved with some slip detected at the walls. At even higher shear rates (above Pe $\sim$ 2.5), the average configuration is that of independent clusters with a liquid-like response, *i.e.* a linear flow profile without slip. Eventually, at the higher shear rates, all clusters are broken down to single particles, as shown in Fig. 3(f). For the $\phi = 0.4$ sample with $U_0 \simeq -20\ k_BT$ this takes place for Pe > 100.

A possible link between gel structure and slip is then the following: as the attraction strength between particles increases, clusters become more compact[42] and the number of contacts between the colloidal network and cell walls decreases, leading to a drop of the apparent friction coefficient. Moreover, rheological measurements and computer simulations[54,65,70] have indicated that low shear rates under no slip conditions promote cluster compaction in order to allow easier flow. Such a mechanism lowers the number of links with the wall during a transient shear period, promoting slip at surfaces that are not strongly attractive or serrated. With increasing $\dot{\gamma}$, the average cluster size decreases and therefore we expect the number of links between the bulk and the wall to increase. Consequently, slip is expected to dominate at low $\dot{\gamma}$ and also high $|U_0|$, due to fewer bonds with the wall as a result of the formation of more compact clusters.

Support for this picture is provided by measurements of the flow curve upon decreasing the shear rate and measuring the stress as a short time average at each shear rate so that there is less time for network formation and steady state to be reached. In Fig. 4 we present a flow curve taken with such rapid decrease of $\dot{\gamma}$ (5 s per point), and compare it with a flow curve taken with increasing $\dot{\gamma}$ where each point is close to steady state. The former exhibits a power law response at low $\dot{\gamma}$ with no measurable yield stress, whereas taking data with longer waiting (green diamond in Fig. 4) shows a departure from the power law and a decrease of the measured stress. This suggests that there is no stress bearing structure and probably the sample consists mainly of flowing independent clusters. On the other hand, when steady state response is reached at each point the flow curve presents a slip stress with the measured stress being lower than that obtained during the rapid measurements. That supports the picture of a yield stress system of interconnected clusters, Fig. 3(a), which however exhibits wall slip, due to a low number of cluster–wall contacts (as a result of shear induced compactification of the clusters) and not of high enough strength. The latter is also responsible for the weaker stress response at low rates compared to the short-time measurement. Nonetheless, we should note that slip has also been detected under low shear rates even immediately after shear rejuvenation, when the sample was much more homogeneous (even close to the wall), than at latter times.

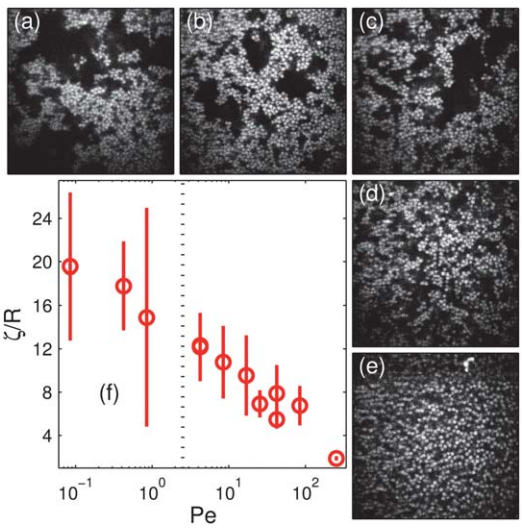

Fig. 3 (a)–(e) Images taken under shear at $z = 5$ μm, and at respectively $\dot{\gamma} = 0.05$, 0.5, 1, 5, and 30 s^{-1} for a suspension at $R = 650$ nm, $\phi = 0.4$, and $U_0 = -20\ k_BT$. (f) Radius of clusters *versus* applied shear rate for fluorescent particles with $R = 650$ nm at $\phi = 0.4$ and $c = 0.5c^*$ (○); the dotted line shows the onset of slip.

3.3 Surface effects and near wall structure

We can take the above idea a step further in order to provide some quantitative predictions. Since slip implies the breaking of links between the bulk and the surface, the slip stress, σ_s, should be related to the number of bulk–wall contacts and their strength and hence indirectly provide an estimation of the

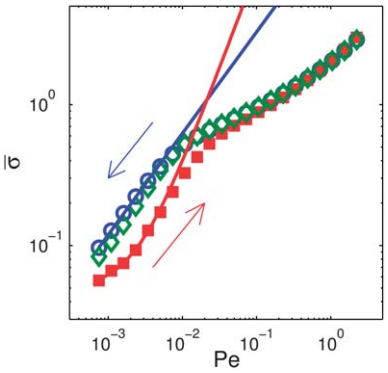

Fig. 4 Normalized flow curves for $R = 138$ nm, $\phi = 0.45$, and $c/c^* = 0.24$ at a decreasing shear rate with a duration of 5 s per point (○) and 30 s per point (◇), and with an increasing shear rate the duration of each point is 30 s (■). The arrows indicate the direction of shear rate change. The continuous lines are the best fit by a Herschel–Bulkley behaviour, the slip stress is 0 Pa for the decreasing shear rate and 0.07 Pa for the increasing shear rate. Flow curves are taken with smooth surfaces.

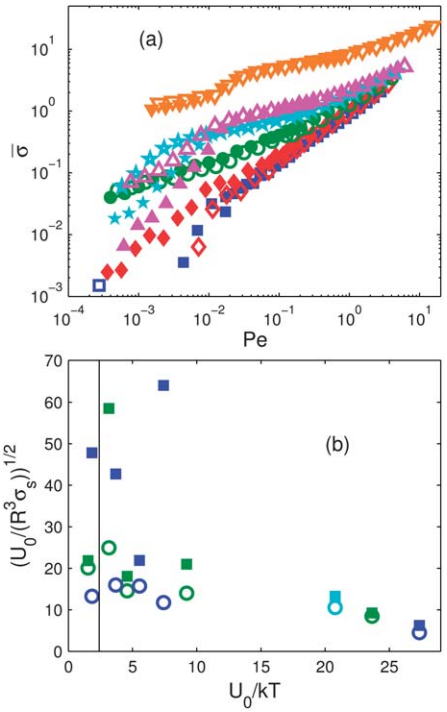

Fig. 5 (a) Normalized flow curves for $\phi = 0.45$, $R = 138$ nm at various attraction strengths $-U_0 = 0$, 2.3, 4.7, 7, 9.4, and 34.6 k_BT (resp. ■, ♦, ●, ★, ▲, ▼), open and close symbols decreasing and increasing shear rates respectively. (b) $\sqrt{|U_0|R^{-3}\sigma_s^{-1}}$ *versus* $|U_0|/k_BT$ for $R = 138$ nm, $\phi = 0.45$ and various polymer concentrations. The open circles use the values of the yield stress going from high to low shear rates, the full squares are the values going from low to high shear rates, the continuous line marks the gel transition. Rheology data are taken with smooth surfaces.

cluster size. In the concentration range studied here we expect clusters close to a surface to form a dense layer resulting in a concentration of surface contacts that scales as ζ^{-2}. Since a layer of particles is attached to the surface by van der Waals and depletion interactions, the clusters are in contact with the surface of the tool *via* particle–particle bonds of energy U_0,[39,51] each of which exerts a force of magnitude $\sim U_0/R$. Consequently, the slip stress should approximately be $\sigma_s = mU_0R^{-1}\zeta^{-2}$, where m is the number of bonds between a cluster and the surface.

Flow curves at various polymer concentrations for suspensions of particles in tetradecane at $\phi = 0.45$ are presented in Fig. 5(a). We can determine the slip stress, σ_s, by fitting the low-$\dot{\gamma}$ portions using eqn (2). In the formula above for σ_s, R is known from light scattering while U_0 is calculated according to the Asakura–Oosawa model modified in ref. 39,51; hence the only unknowns are m and ζ. Since the clusters end up being compact we can assume $m \simeq 1$. The results are plotted in Fig. 5(b), where we compare the cluster size estimated by $\sqrt{U_0R^{-3}\sigma_s^{-1}} \simeq \zeta/R$ at a constant volume fraction $\phi = 0.45$ for the various attraction strengths represented by the data in Fig. 5(a).

We notice that once the gel line is crossed the cluster size decreases upon further increase of the attraction strength, Fig. 5(b). As mentioned earlier, this is consistent with light scattering and optical microscopy findings of gels at rest[42] and can be explained by a contraction of the clusters at low shear rates or with increasing attraction. As the clusters become bigger and more compact ζ increases and m decreases, hence σ_s should decrease. We also note that as the polymer concentration is increased, the difference in σ_s between flow curves taken from low to high shear rate or the opposite is less pronounced.

Together with the data in Fig. 4, this suggests the following picture for the time evolution of the network. During rejuvenation at high shear rates each colloid is independent, no network is formed and no slip is present. After high shear is stopped, as the sample ages a loose network is formed. Because of the network the sample now presents a yield stress and a competition between yielding and slip begins; this leads to slip and the presence of a measurable slip stress. As time passes the size of the aggregates increases resulting in a decrease of the slip stress and finally aggregates compact and σ_s further decreases. Moreover, close to the walls one may also reasonably expect that a layer of lower density could be formed, as particles cannot achieve optimal configuration there. Such a low-density layer would then be less viscous and therefore should be sheared stronger than the bulk, leading to the formation of a high shear rate band near the wall as seen in Fig. 2(b) near the cone surface at the lowest rates.

3.4 A slip state diagram

Varying ϕ, c_p, R and the solvent, we monitored the slip behaviour throughout state space, Fig. 6. The solid line indicates the gel boundary as determined previously.[39,51] To facilitate comparison between systems with different ξ, we normalize the interparticle attraction by its strength at the gel transition. With very few exceptions (for which see Section 3.5), slip only occurs in the gel regime (zone II in Fig. 6), while neither liquids (zone I) nor glasses (zone III) exhibit any slip when the tool's surfaces are coated, in agreement with previous studies on repulsive[10] and attractive[48] glasses where coated walls or particles dispersed in non-index matching solvents[67] were used. Note that in agreement with previous work,[67] measurements in concentrated

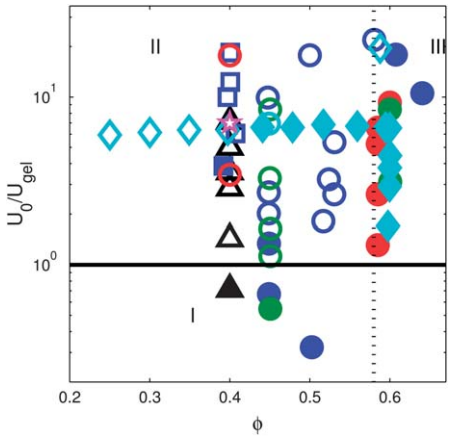

Fig. 6 Suspension behaviour at low shear rates: open symbols indicate slip whereas solid symbols no slip. The shape and color of the symbols define the sample (see Table 1). ♦ (data from ref. 48), ■ (data from ref. 24), △ extracted from ref. 20. All energy is normalized by the gelation energy. The dotted line shows $\phi = 0.58$.

liquid samples reveal the same behavior (Fig. 7), as G' and G'' exhibit a delayed drop with waiting time, indicative of the onset of slip, only for samples with significant attractions.

It is striking that at high c_p (or, equivalently, large enough $|U_0|$), slip seems to be present even when particle coated surfaces are used, provided that $\phi \lesssim \phi_g \approx 0.58$, *i.e.* below the glass transition. In other words, one of our main findings is that for gels at intermediate and low ϕ, surface roughness of the order of the particle size is not sufficient to inhibit slip. For such systems with structural inhomogeneities (clusters) of several particle radii, the only way to avoid slip is to use serrated tools with roughness of the order of few hundreds of μm, which is at least one order of magnitude larger than the structural inhomogeneities present in the sample. Note that these findings are robust: they are reproducible with respect to changes in the measurement protocol (controlled strain or stress), tool geometry (cone–plates of different sizes), and the origin of surface roughness on the single-particle level (deliberately coated or from van der Waals attraction due to non-index matching).

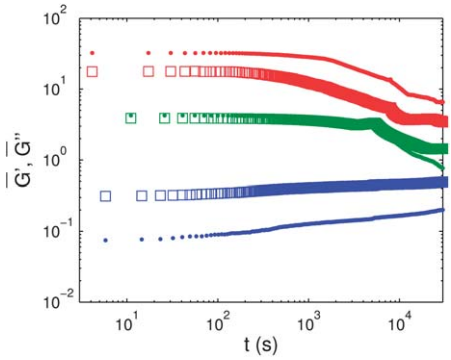

Fig. 7 G' and G'' (respectively ●, □) *versus* time for $R = 138$ nm, $\xi = 0.1$, and $\phi = 0.45$ suspensions at various polymer concentrations in tetradecane. $-U_0 = 0$, 7, and 34.6 k_BT (respectively ●, □, ●, □, ●, □).

3.5 Polydispersity effects

Fig. 6 shows that a small number of samples in the gel regime do not slip. We suggest that the commonality between these samples is high polydispersity. Fig. 8(a) and (b) show the flow curves and the time evolution of G' and G'' for two suspensions at the same ϕ (=0.45) and c_p in the same solvent (*cis*-decalin) but with different particle polydispersity. Whereas at high $\dot{\gamma}$ the flow curves are nearly identical, at low $\dot{\gamma}$ the less polydisperse sample ($p = 15\%$) shows the stress drop characteristic of slip while the more polydisperse one ($p = 24\%$) continued to follow HB behaviour to the lowest stresses probed. The time evolution of G' and G'' presents a similar picture. Whereas the more polydisperse sample exhibits the expected rheological ageing of a strengthening gel with continuously increasing and decreasing G' and G'' respectively, the G' of the less polydisperse sample drops below G'' after two minutes (*cf.* Fig. 1(b)).

The origins of suppression of slip by polydispersity could perhaps be traceable back to the R-dependence of the depletion effect – non-adsorbing polymers induce lower attraction between smaller particles than larger ones as U_0 scales as ξ^{-1}. It is therefore possible that in a polydisperse system, some of the smallest particles are not incorporated into the gel network, but remain free. This may have two effects: lowering σ_y, eqn (1), of the gel network by lowering its effective concentration, and increasing the slip stress σ_s, eqn (2), by increasing the viscosity of the effective suspending medium, which is now a dispersion of small particles rather than the pure solvent. Another

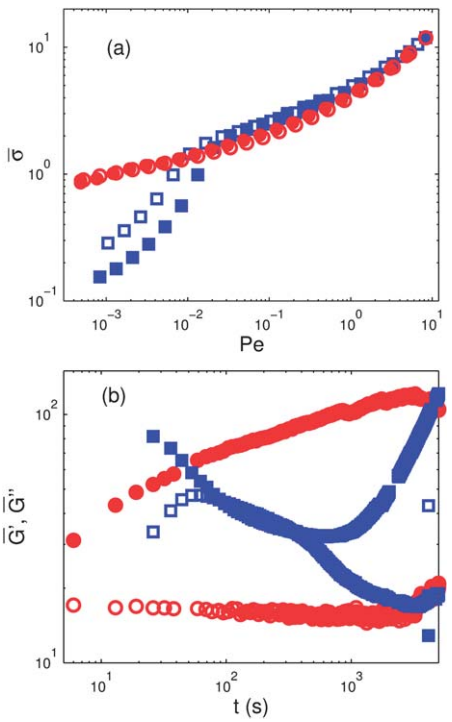

Fig. 8 (a) $\bar{\sigma}$ *versus* Pe for $R = 138$ nm, $\phi = 0.45$, and $U(0) = -18$ k_BT in *cis*-decalin with $p = 15\%$ (□) and $p = 24\%$ (○) with coated surfaces in both cases; open symbols: going from high to low shear rates; plain symbols: going from low to high shear rates. (b) $\bar{G}'$ and $\bar{G}''$ *versus* time with polydispersity $p = 15\%$ (resp. filled and open □) and polydispersity $p = 24\%$ (resp. filled and open ○).

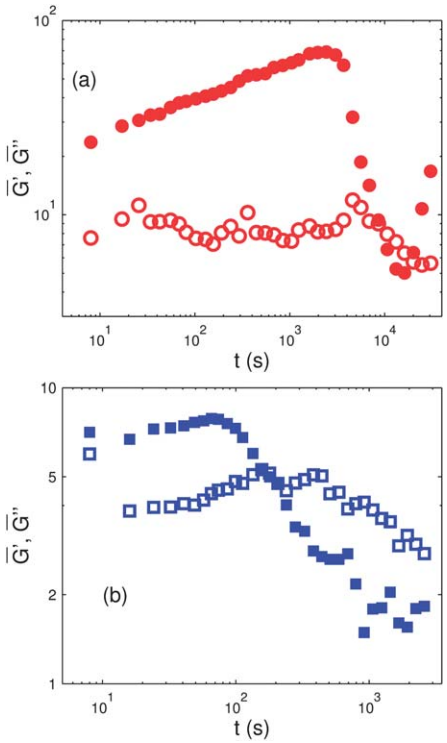

Fig. 9 (a) $\bar{G}'$ and $\bar{G}''$ *versus* time (filled and open symbols respectively) for samples with $p = 24\%$ and $U_0 = -18\ k_BT$. (a) $\phi = 0.35$, (b) $\phi = 0.25$.

possibility is that the smaller particles experiencing lower attractions would have higher mobility that would lead to increased contact with the surface and therefore reduce slip.

Interestingly, the polydispersity effect on slip is ϕ-dependent. Fig. 9 shows the time dependence of G' and G'' for the $p = 24\%$ system at two concentrations lower than the $\phi = 0.45$ sample already discussed, but with the same U_0. These samples, at $\phi = 0.35$ and 0.25, show clear evidence of slip with G' becoming lower than G'' after a certain characteristic time which is smaller for smaller volume fractions. This enhancement of slip is different from what is observed in the case of concentrated hard spheres, where slip disappears as ϕ is lowered from glassy towards fluid states.[67]

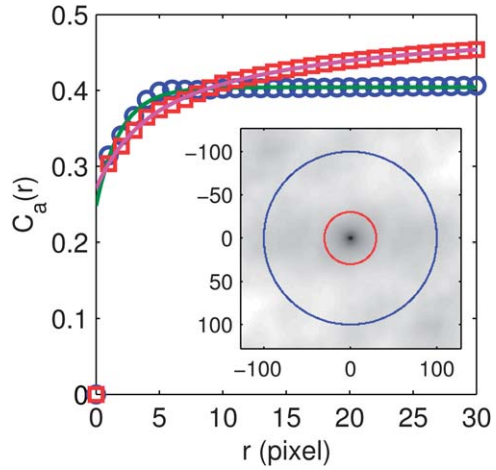

Fig. 10 $C_a(r)$ for $\dot{\gamma} = 1\ s^{-1}$ (○) and $\dot{\gamma} = 30\ s^{-1}$ (○), the magenta and green lines are the respective fit by eqn (4). Inset $C_a(x, y)$ at $\dot{\gamma} = 1\ s^{-1}$, the blue dots mark the points used for $r = 100$, the red dots for $r = 30$.

4 Conclusions

In this paper we showed that attractive gels slip under shear when the attraction between particles is high enough, even for surfaces of roughness similar to the particle size. Slip is caused by the reduction of the number of bonds between bulk and surface as the cluster size increases. One must use tools with roughness orders of magnitude larger than the particle size to effectively prevent slip. This phenomenon should be expected in every aggregating system such as attractive colloidal suspensions[35] or emulsions.[36] It clearly highlights, in agreement with previous studies,[10,71] that even model systems present complex behaviour at surfaces and that special care should be taken when interpreting rheological data from complex multi-component fluids. Caution must also be exercised in choosing the roughness of the geometry used to ensure no-slip conditions. Moreover, particle–particle interactions are of significant importance as evidenced by the difference between slip in attractive and repulsive suspensions.[10,72,73] In the latter the bulk remains unchanged while slip is taking place at the surface. In contrast, in the present experiments, slip is also closely related with changes in the bulk structure as a function of shear rate; a liquid whose behaviour is dominated by single particle dynamics at high shear rates is replaced by independent or interconnected clusters that dominate the surface–bulk interactions at low shear rates.

On the application side, slip phenomena are ubiquitous in a wide range of commercial products and industrial processes from multiphase food products such as molten chocolate[74] to flow of construction materials such as concrete and cement pastes.[75,76] Flow curves in such systems commonly exhibit a sudden drop of the effective viscosity with increasing shear rate (or applied stress) similar to that observed in model attractive colloids such as those presented here (Fig. 1) and elsewhere.[20] Therefore the understanding of the micro- and mesoscopic structure and of wall–particle interactions and their dependence on shear rate may allow optimization of production and mechanical properties at will.

A Determination of cluster size

To determine cluster sizes, we auto-correlate each image:

$$C_a(p,\ m) = \left\langle (I(n,\ x,\ y) - I(n,\ x-p,\ y-m))^2 \right\rangle_{n,x,y}, \qquad (3)$$

where $I(n, i, j)$ is the intensity of pixel i, j of the n^{th} image and $\langle \ldots \rangle_{n,x,y}$ denotes averaging over pixels and images, and $C_a(0) = 0$. The pixel position $(p,\ m)$ is converted to a distance r by averaging over all pixels such that $r - 0.5 < \sqrt{p^2 + m^2} < r + 0.5$, *i.e.*, we take $C_a(r) = \langle C_a(p,\ m) \rangle_{\sqrt{p^2+m^2} \in [r-0.5; r+0.5]}$.

For most $\dot{\gamma}$, $C_a(r)$ presents a two-step increase (see Fig. 10). The exception is that at the highest $\dot{\gamma}$, where a single step increase is observed. The first step in the rise of $C_a(r)$ away from

$r = 0$ is similar at all $\dot{\gamma}$, and is determined by the particle size. The correlation begins to drop beyond displacements of order R. A second rise in $C_a(r)$ corresponds to either the cluster size or the size of the 'holes' between clusters, or, more precisely, the smaller of the two. To estimate the cluster size, we fit $C_a(r)$ by:

$$C_a(r) = a - b\exp(-r/l_0) - c\exp(-r/l). \quad (4)$$

where l_0 is the radius of the colloid R in pixels. Of the four remaining fitting parameters, (a, b, c, l), it is the last that has the most obvious physical interpretation: l is either the cluster size or the void size depending on ϕ; but we expect the two to scale proportionately. We simply convert l into a physical length, ζ, and use it to estimate the cluster size. For the highest shear rate, $C_a(r)$ presents a single step, which we fit with eqn (4) to provide an estimate of the particle size.

The error bars in Fig. 3(f) were estimated by measuring the cluster size at three different heights: 5 μm from the glass plate, the center of the cell and 5 μm from the cone.

Acknowledgements

We thank A.B. Schofield for particle synthesis and sizing. RB and WCKP were funded by EP/D067650. GP, NK and PB acknowledge EU funding through ToK'Cosines' (MTCD-CT-2005-029944) and FP7-Infrastructures 'ESMI' (CP&CSA-2010-262348).

References

1 M. Mooney, *J. Rheol.*, 1931, **2**, 210–222.
2 A. Yoshimura and R. K. Prud'homm, *J. Rheol.*, 1988, **32**, 53–67; A. Yoshimura and R. K. Prud'homme, *J. Rheol.*, 1988, **32**, 575–584.
3 H. A. Barnes, *J. Non-Newtonian Fluid Mech.*, 1995, **56**, 221–251.
4 C. Neto, D. R. Evans, E. Bonaccurso, H.-J. Butt and V. S. J. Craig, *Rep. Prog. Phys.*, 2005, **68**, 2859–2897.
5 J.-L. Barrat and L. Bocquet, *Phys. Rev. Lett.*, 1999, **82**, 4671–4674.
6 Y. Zhu and S. Granick, *Phys. Rev. Lett.*, 2001, **87**, 096105; *Phys. Rev. Lett.*, 2002, **88**, 106102.
7 S. G. Hatzikiriakos and J. M. Dealy, *J. Rheol.*, 1991, **35**, 497–523.
8 F. Brochardt and P. G. de Gennes, *Langmuir*, 1992, **8**, 3033–3037.
9 L. Léger, H. Hervet, G. Massey and E. Durliat, *J. Phys.: Condens. Matter*, 1997, **9**, 7719–7740.
10 P. Ballesta, R. Besseling, L. Isa, G. Petekidis and W. C. K. Poon, *Phys. Rev. Lett.*, 2008, **101**, 258301.
11 U. Yilmazer and D. M. Kalyon, *J. Rheol.*, 1989, **33**, 1197–1212.
12 D. M. Kalyon, *J. Rheol.*, 2005, **49**, 621–640.
13 S. C. Jana, B. Kapoor and A. Acrivos, *J. Rheol.*, 1995, **39**, 1123–1132.
14 I. Cohen, B. Davidovitch, A. B. Schofield, M. P. Brenner and D. A. Weitz, *Phys. Rev. Lett.*, 2006, **97**, 215502.
15 F. Soltani and U. Yilmazer, *J. Appl. Polym. Sci.*, 1998, **70**, 515–522.
16 L. Isa, R. Besseling and W. C. K. Poon, *Phys. Rev. Lett.*, 2007, **98**, 198305.
17 H. Wassenius and P. T. Callaghan, *Eur. Phys. J. E: Soft Matter Biol. Phys.*, 2005, **18**, 69–84.
18 J. Persello, A. Magnin, J. Chang, J.-M. Piau and B. Cabane, *J. Rheol.*, 1994, **38**, 1845–1870.
19 T. Gibaud, C. Barentin and S. Manneville, *Phys. Rev. Lett.*, 2008, **101**, 258302.
20 R. Buscall, *et al.*, *J. Rheol.*, 1993, **37**, 621–641.
21 W. B. Russel and M. C. Grant, *Colloids Surf., A*, 2000, **161**, 271–282.
22 T. Gibaud, C. Barentin, N. Taberlet and S. Manneville, *Soft Matter*, 2009, **5**, 3026–3037.
23 T. Gibaud, D. Frelat and S. Manneville, *Soft Matter*, 2010, **6**, 3482–3488.
24 M. Laurati, S. U. Egelhaaf and G. Petekidis, *J. Rheol.*, 2011, **55**, 673–706.
25 H. J. Walls, S. B. Caines, A. M. Sanchez and S. A. Khan, *J. Rheol.*, 2003, **47**, 847–868.
26 V. Bertola, F. Bertrand, H. Tabuteau, D. Bonn and P. Coussot, *J. Rheol.*, 2003, **47**, 1211–1226.
27 H. M. Princen, *J. Colloid Interface Sci.*, 1985, **105**, 150–171.
28 S. P. Meeker, R. T. Bonnecaze and M. Cloitre, *Phys. Rev. Lett.*, 2004, **92**, 198302.
29 J.-B. Salmon, S. Manneville, A. Colin and B. Pouligny, *Eur. Phys. J.: Appl. Phys.*, 2003, **22**, 143–154; *Eur. Phys. J. E*, 2003, **10**, 209–221.
30 G. Katgert, M. E. Móbius and M. van Hecke, *Phys. Rev. Lett.*, 2008, **101**, 058301.
31 H. Hu, R. G. Larson and J. J. Magda, *J. Rheol.*, 2002, **46**, 1001–1021.
32 M. P. Lettinga and S. Manneville, *Phys. Rev. Lett.*, 2009, **103**, 248302.
33 R. Besseling, L. Isa, P. Ballesta, G. Petekidis, M. E. Cates and W. C. K. Poon, *Phys. Rev. Lett.*, 2010, **105**, 268301.
34 J. Buscall, *J. Rheol.*, 2010, **54**, 1177–1183.
35 D. F. K. Hughes and I. D. Robb, *Langmuir*, 1999, **15**, 8795–8799.
36 R. Pal, *Chem. Eng. Commun.*, 1990, **98**, 211–222; R. Pal, *Ind. Eng. Chem. Res.*, 1998, **37**, 2052–2058.
37 R. Besseling, L. Isa, E. R. Weeks and W. C. K. Poon, *Adv. Colloid Interface Sci.*, 2009, **146**, 1–17.
38 S. Asakura and F. Oosawa, *J. Polym. Sci.*, 1958, **33**, 183–192.
39 D. G. A. L. Aarts, R. Tuinier and H. N. W. Lekkerkerker, *J. Phys.: Condens. Matter*, 2002, **14**, 7551–7561.
40 K. N. Pham, A. M. Puertas, J. Bergenholtz, S. U. Egelhaaf, A. Moussaid, P. N. Pusey, A. B. Schofield, M. E. Cates, M. Fuchs and W. C. K. Poon, *Science*, 2002, **296**, 104–106.
41 V. Prasad, V. Trappe, A. D. Dinsmore, P. N. Segre, L. Cipelletti and D. A. Weitz, *Faraday Discuss.*, 2003, **123**, 1–12.
42 M. Laurati, G. Petekidis, N. Koumakis, F. Cardinaux, A. B. Schofield, J. M. Brader, M. Fuchs and S. U. Egelhaaf, *J. Chem. Phys.*, 2009, **130**, 134907.
43 X. Ye, T. Narayanan, P. Tong, J. S. Huang, M. Y. Lin, B. L. Carvalho and L. J. Fetters, *Phys. Rev. E: Stat. Phys., Plasmas, Fluids, Relat. Interdiscip. Top.*, 1996, **54**, 6500–6510.

44 A. Muratov, A. Moussaid, T. Narayanan and E. I. Kats, *J. Chem. Phys.*, 2009, **131**, 054902.
45 C. P. Royall, S. R. Williams, T. Ohtsuka and H. Tanaka, *Nat. Mater.*, 2008, **7**, 556–561.
46 P. Varadan and M. J. Solomon, *J. Rheol.*, 2003, **47**, 943–968.
47 C. J. Dibble, M. Kogan and M. J. Solomon, *Phys. Rev. E: Stat., Nonlinear, Soft Matter Phys.*, 2006, **74**, 041403; C. J. Dibble, M. Kogan and M. J. Solomon, *Phys. Rev. E: Stat., Nonlinear, Soft Matter Phys.*, 2008, **77**, 050401.
48 K. N. Pham, G. Petekidis, D. Vlassopoulos, S. U. Egelhaaf, P. N. Pusey and W. C. K. Poon, *Europhys. Lett.*, 2006, **75**, 624–630; K. N. Pham, G. Petekidis, D. Vlassopoulos, S. U. Egelhaaf, P. N. Pusey and W. C. K. Poon, *J. Rheol.*, 2008, **52**, 649–676.
49 S. A. Shah, Y.-L. Chen, K. S. Schweizer and C. F. Zukoski, *J. Chem. Phys.*, 2003, **119**, 8747–8760.
50 W. C. K. Poon, *J. Phys.: Condens. Matter*, 2002, **14**, R859–R880.
51 J. Bergenholtz, W. C. K. Poon and M. Fuchs, *Langmuir*, 2003, **19**, 4493–4503.
52 P. J. Lu, J. C. Conrad, H. M. Wyss, A. B. Schofield and D. A. Weitz, *Phys. Rev. Lett.*, 2006, **96**, 028306.
53 S. Ramakrishnan, Y.-L. Chen, K. S. Schweizer and C. F. Zukoski, *Phys. Rev. E: Stat., Nonlinear, Soft Matter Phys.*, 2004, **70**, 040401(R).
54 N. Koumakis and G. Petekidis, *Soft Matter*, 2011, **7**, 2456–2470.
55 K. Kroy, M. E. Cates and W. C. K. Poon, *Phys. Rev. Lett.*, 2004, **92**, 148302.
56 P. J. Lu, E. Zaccarelli, F. Ciulla, A. B. Schofield, F. Sciortino and D. A. Weitz, *Nature*, 2008, **453**, 499–503.
57 E. Zaccarelli, P. J. Lu, F. Ciulla, D. A. Weitz and F. Sciortino, *J. Phys.: Condens. Matter*, 2008, **20**, 494242.
58 E. Zaccarelli and W. C. K. Poon, *Proc. Natl. Acad. Sci. U. S. A.*, 2009, **106**, 15203–15208.
59 H. Tanaka and T. Araki, *Europhys. Lett.*, 2007, **79**, 58003.
60 W. Schaertl and H. Sillescu, *J. Stat. Phys.*, 1994, **77**, 1007–1025.
61 G. Bryant, S. R. Williams, L. Qian, I. K. Snook, E. Perez and F. Pincet, *Phys. Rev. E: Stat., Nonlinear, Soft Matter Phys.*, 2002, **66**, 060501.
62 D. B. Hough and L. R. White, *Adv. Colloid Interface Sci.*, 1980, **14**, 3–41.
63 W. Sigmund, G. Pyrgiotakis and A. Dage, in *Chemical Processing of Ceramics*, ed. B. Lee and S. Komarneni, CRC Press, 2nd edn, 2005, ch. 11, pp. 271–277.
64 D. Bonn, H. Tanaka, P. Coussot and J. Meunier, *J. Phys.: Condens. Matter*, 2004, **16**, S4987–S4992.
65 N. Koumakis, PhD thesis, University of Crete, 2011.
66 V. A. Tolpekin, M. H. G. Duits, D. van den Ende and J. Mellema, *Langmuir*, 2004, **20**, 2614–2627.
67 P. Ballesta, G. Petekidis, L. Isa, W. C. K. Poon and R. Besseling, *J. Rheol.*, 2012, **56**, 1005–1037.
68 J.-M. Condre, C. Ligoure and L. Cipelletti, *J. Stat. Mech.: Theory Exp.*, 2007, P02010.
69 S. W. Kamp and M. L. Kilfoil, *Soft Matter*, 2009, **5**, 2438–2447.
70 (*a*) N. Koumakis, *PhD Thesis*, University of Crete, 2011; (*b*) N. Koumakis, P. Ballesta, R. Besseling, W. C. K. Poon, J. F. Brady and G. Petedikis, *SDCS2012 conference proceedings*, AIP, 2013.
71 R. Besseling, E. R. Weeks, A. B. Schofield and W. C. K. Poon, *Phys. Rev. Lett.*, 2007, **99**, 028301.
72 Y. C. Lam, Z. Y. Wang, X. Chen and S. C. Joshi, *Powder Technol.*, 2007, **177**, 162–169.
73 R. Seth, R. T. Bonnecaze and M. Cloitre, *J. Rheol.*, 2008, **52**, 1241–1268.
74 J. E. Taylor, I. Van Damme, M. L. Johns, A. F. Routh and D. I. Wilson, *J. Food Sci.*, 2009, **74**, 55–61.
75 R. J. Mannheimer, *J. Rheol.*, 1991, **35**, 113–133.
76 A. W. Saak, H. M. Jenningsa and S. P. Shah, *Cem. Concr. Res.*, 2001, **31**, 205–212.